

Evolution of Accretion Disc Geometry of GRS 1915+105 during its χ state as revealed by TCAF solution

Broja G. Dutta,^{1,2*} Partha Sarathi Pal,^{3†} and Sandip K. Chakrabarti^{4,2‡}

¹Department of Physics, Rishi Bankim Chandra College, Naihati, W.B, 743165, India.

²Indian Centre for Space Physics, Kolkata, 700084, India.

³Sun Yat-sen University, 135 West Xingang Road, Guangzhou, 510275, China.

⁴S. N. Bose National Centre For Basic Sciences, Kolkata, 700098, India.

Accepted XXX. Received YYY; in original form ZZZ

ABSTRACT

The evolution of the C-type low frequency quasi-periodic oscillations (LFQPOs) and associated time lag in transient black hole sources as a function of time can be explained by variation of the Compton cloud size in a Two Component Advective Flow solution (TCAF). A similar study of a persistent source, GRS 1915+105, has not been attempted. We fit the evolution of QPOs with propagatory oscillating shock (POS) solution for two sets of so-called χ -state observations and find that the shock steadily recedes with almost constant velocity when QPO frequency is decreasing and the spectrum is hardening. The shock moves inward with a constant velocity $v_0 = 473.0$ cm s⁻¹ and $v_0 = 400.0$ cm s⁻¹ respectively in these two cases, when the QPO frequency is increasing and the spectrum softens. This behavior is similar to what was observed in XTE J1550-564 during the 1998 outburst. The time lag measured at the QPO frequency varies in a similar way as the size of the Compton cloud. Most interestingly, in both the cases, the lag switches sign (hard lag to soft lag) at a QPO frequency of $\sim 2.3 - 2.5$ Hz irrespective of the energy of photons. We find, at very low frequencies < 1 Hz, the Comptonizing Efficiency (CE) increases with QPO frequency and at higher QPO frequencies the trend is opposite. The time lags become mostly positive at all energies when CE is larger than $\sim 0.85\%$ for both the sources.

Key words: accretion, accretion discs – radiation: dynamics – shock waves – stars: black holes

1 INTRODUCTION

The Galactic black hole X-ray binary GRS 1915+105 has been persistently bright since its discovery in 1992 (Remillard & McClintock 2006). This source exhibits complex timing and spectral variability properties which are different from other compact binary sources and hence difficult to interpret within the standard framework. Diverse variability patterns (Greiner et al. 1996; Hannikainen et al. 2005; Klein-Wolt et al. 2002) in X-rays are classified into 12 separate classes based on the nature of the light curves and color-color diagrams. Each of these variability classes is then reduced into three basic states, namely, A, B, and C (see also Markwardt et al. 1999; Munro et al. 1999). According to these authors, the state ‘C’ is a low-luminosity and spectrally hard state while the states B and A both are

high and spectrally soft state. They differ only in luminosity while B state is related to high-luminosity and A state is related low-luminosity (Klein-Wolt et al. 2002). Generally, the state C lasts for a few weeks to months and belongs to the so-called χ variability class, which is equivalent to a standard “low hard state” (LHS). In this state, strong type-C QPOs are observed often evolving with time in the range 0.5–10 Hz (Markwardt et al. 1999; Trudolyubov et al. 1999; Reig et al. 2000). The complex timing behavior certainly challenges models which predict both the X-ray variability and the X-ray spectra (Munro et al. 2001). It is suggested that these LFQPOs must be linked to the properties of the accretion disk since their centroid frequencies are correlated with the disk flux (Markwardt et al. 1999) while the emitted luminosity itself varies, for example due to changes in mass accretion rate (Tagger & Pellat 1999; Cabanac et al. 2010). In Chakrabarti & Manickam (2000); Vadawale et al. (2001); Rao et al. (2000); Chakrabarti et al. (2005) it was shown that the Comptonized photons produce QPOs and thus they are intrinsically related to spectral states.

* E-mail: brojadutta@gmail.com

† E-mail:

parthasarathi.pal@gmail.com

‡ E-mail: chakraba@bose.res.in

parthasp@mail.sysu.edu.cn;

There are several models in the literature which attempt to explain origins of QPOs. A possible origin of the type-C QPOs could be Lens-Thirring precession of the Comptonizing medium, due to misalignment of the black hole spin and the inner accretion flow (Stella & Vietri 1999; Stella et al. 1999; Ingram et al. 2009). Heil et al. (2015); Motta et al. (2015) confirmed that the QPO amplitude depends on the inclination of the binary orbit, strongly suggesting a geometric origin (Schnittman et al. 2006). Ingram & van der Klis (2015) studying QPO phase-resolved spectra, found that the iron line equivalent width changes over a QPO cycle in GRS 1915+105, strongly pointing to a geometric origin. Meanwhile Molteni et al. (1996); Chakrabarti et al. (2004); Garain et al. (2014); Chakrabarti et al. (2015) suggested that these QPOs could be related to the resonance oscillation of the Compton clouds since their occurrences strongly depend on the accretion rates which in turn change the cooling time scale. This latter solution was demonstrated by complete hydrodynamic simulations and does not require a spinning black hole.

The energy dependence of QPOs in GRS 1915+105 has been studied by Chakrabarti & Manickam (2000); Qu et al. (2010); Yan et al. (2013). Chakrabarti & Manickam (2000) found that the RMS amplitude increases with energy. Yan et al. (2013) also found a smooth evolution of the dependence of QPO frequency on photon energy. In XTE J1550-564, for frequencies above ~ 3.2 Hz, (Li et al. 2013) found an increase in QPO frequency with energy and below ~ 3.2 Hz no variations with energy were observed. The energy dependence of time/phase lags has been studied by (Cui 1999; Reig et al. 2000; Qu et al. 2010; Pahari et al. 2013). They found a smooth relation between the time/phase lag and energy in GRS 1915+105. A similar behavior is also found in XTE J1550-564 (Wijnands et al. 1999; Cui et al. 2000). Qu et al. (2010) observed that the slope of this energy dependent curve is positive when hard lags are observed and the slope is negative when soft lags are observed with the lag changing sign from positive to negative at ~ 2 Hz. The existence of such a crossover frequency is of particular interest. In this paper we show that in GRS 1915+105 this frequency remains the same for different intervals of χ variability class observation (hard state) of GRS 1915+105. In the case of XTE J1550-564, the lag switches at a QPO frequency ~ 3.2 Hz (Dutta & Chakrabarti 2016) which is also unique. This unique feature, which appears to characterize high inclination galactic black hole candidates (GBHs) can be understood only through proper understanding of the flow geometry. The time lags were first explained to be due to the Comptonization of soft seed photons by hot electrons, known as ‘Compton reverberation’ (Payne 1980; Miyamoto et al. 1988) which naturally produces hard time lags. Several models are proposed (see Cui 1999; Poutanen 2001, for review and references therein) to explain the hard and soft lags associated with QPOs observed in Galactic binary systems. According to propagating perturbation model Böttcher & Liang (1999); Lin et al. (2000), it is not clear how the propagation direction changes when the QPO frequency is close to the crossover frequency when the phase lag of the QPO changes sign. Noble et al. (2011) reproduced the observed time lags in the continuum during the ‘plateau’ regions of GRS 1915+105 by invoking a tempera-

ture stratification in a corona and assuming that the optical depth of the Comptonizing region increases as the disk inner radius moves inward. In GRS 1915+105, Vierdayanti et al. (2013) pointed out that self-occultation effects for the high inclination (Mirabel & Rodríguez 1994) source could play an important role in the observed variation of X-ray flux. The reason why these models may fail to explain this behavior in totality is that they do not account for the fact that the time/phase lags could be due to multiple origins (Dutta & Chakrabarti 2016) and what we are observing is the resultant of many such causes.

The inclination of the source could be an important parameter while studying the properties of QPO and time lag. Using Monte-Carlo simulations, Ghosh et al. (2011) found that for the same disk flow parameters, the spectrum is hardened when the inclination angle is increased. This was later confirmed by Muñoz-Darias et al. (2013) also. Heil et al. (2015) took 12 transient LMXBs (excluding GRS 1915+105) and considered hard and hard-intermediate states, and found that in higher inclination systems, there is systematically harder X-ray power-law emission. Thus, the inclination affects the ratio of the hard and soft photons, time lag and QPO amplitude.

Despite these efforts to explain the LFQPOs and their evolution and origin of the lags, none appears to be able to explain the cross over of lags for a particular source at the fixed QPO frequency, such as, $\sim 2.3 - 2.5$ Hz in GRS 1915+105 or ~ 3.2 Hz in XTE J1550-564 both of which have a similar (high) inclination angle (Orosz et al. 2011). Earlier, the Two Component Advective Flow (TCAF) solution was used to explain the QPO behavior (Rao et al. (2000); Chakrabarti et al. (2009); Debnath et al. (2010); Nandi et al. (2012); Molla et al. (2016, 2017), etc.), spectral properties (Smith et al. (2002); Wu et al. (2002); Choudhury & Rao (2004); Pottschmidt et al. (2006); Smith et al. (2007); Cambier & Smith (2013); Debnath et al. (2015); Mondal et al. (2014); Chatterjee et al. (2016), etc.), CE variation (Pal et al. 2013; Pal & Chakrabarti 2014) and time-lag properties (Dutta & Chakrabarti 2016) in BH binary systems during outbursts. In TCAF paradigm which originates from self-consistent transonic flow solution, the equatorial plane has a standard Keplerian disk and the sub-Keplerian (i.e., lower angular momentum) halo surrounds it. CENtrifugal pressure supported BOUNDary Layer or CENBOL is also formed between inner and outer sonic points which plays the role of the Compton cloud. Only in TCAF, the Compton cloud (i.e., CENBOL) is self-consistently reduced in size as the soft state is approached and QPO frequency is increased, and thus the time lag properties are self-consistently linked to the spectral properties. Other models, such as the the disk corona model (Haardt & Maraschi 1993; Zdziarski et al. 2003) and the lamp-post models (Martocchia & Matt 1996; Miniutti & Fabian 2004) are yet to address all the observed complex aspects within a single framework..

In the POS model (Chakrabarti et al. 2008, 2009; Debnath et al. 2010; Garain et al. 2014), the resonance oscillation of the post-shock region, i.e., the Compton cloud, causes the observed low-frequency quasi-periodic oscillations (QPOs). The evolution of QPO frequency is explained by the systematic variation of mean size of the Compton cloud, i.e.,

the steady radial movement of the shock front. It moves inwards when the CENBOL is cooled down. Opposite is true when it is heated (Mondal et al. 2015). As the shock moves in with the increase in disk accretion rate, the density and optical depth also generally increases. Thus, analysis of the energy-dependent temporal properties in different variability timescales can diagnose the dynamics and geometry of accretion flows around black holes. This has been shown for the high inclination transient black hole source XTE J1550-564 during its 1998 outburst and the low-inclination black hole transient source GX 339-4 during its 2006-07 outburst using RXTE/PCA data (Dutta & Chakrabarti 2016). However, the dependence of lag on photon energy is more intriguing. GX 339-4 was found to exhibit only the positive lag for all QPO frequencies, while in XTE J1550-564, the lag switches sign and becomes negative at a crossing frequency of ~ 3.2 Hz (Dutta & Chakrabarti 2016). It was explained qualitatively by adding up variations of the lag components at different length scales (Dutta & Chakrabarti 2016). The lag is observed in one band with respect to the other band. But in each energy band the photons are coming from different physical processes such as Compton scattering, reflection, focusing by curved space time, even due to down-scattering etc. Therefore the observed lag will depend on the relative contribution of the different processes in that energy bin. In a soft-lag, the soft photons are delayed due to the longer path or the delayed hard photons are down scattered to softer energies. In a high inclination system the soft lags might also be due to a dominant reflection component. This effect is opposite in a low inclination system. Thus the delay will depend on the inclination angle (Chatterjee et al. 2017; Dutta & Chakrabarti 2016). The dependence on QPO frequency is a consequence of the frequencies being dependent on CENBOL size which in turn determines the fraction of photons which can reach the observer when inclination is high (obscuration effect). At a given CENBOL size scale the lag changes its sign. This frequency is not universal as the dominating lag would depend on the inclination angle and the mass of the black hole which determines the length scales of the Compton cloud.

In case of the variable source GRS 1915+105 which is continuously active in X-rays since its discovery, Pal et al. (2011) observed that the average size of Comptonizing region (i.e., CENBOL) changes in a well defined way as it transits from one variability class to another. Using Comptonizing Efficiency (CE) which is the ratio of number of power-law photons to the number of blackbody photons in the spectrum at any given instant, they sequence the different classes according to the monotonic changes in CE or geometry. Thus our goal is to study the evolution of temporal properties of GRS 1915+105 and compare with those obtained in the transient sources.

In the present paper, we extend the earlier studies of Dutta & Chakrabarti (2016) applied to transient sources to the persistent X-ray source GRS 1915+105, to understand the behavior of its time/phase-lag properties and evolution of accretion geometry by fitting QPO evolution with POS solution. We study the evolution of QPO frequency, time lag and CE. We specially choose long duration hard state or state C where the variability properties (such as QPOs and time lag in sub-second scale) can be easily studied. We study these properties in GRS 1915+105 and compare

with the other high inclination black hole candidate (BHC), XTE J1550-564 which exhibit frequent outburst phases. We also calculate the QPO cross over frequency for different energy bands. We interpret the results by using the changes in geometry within this hard state as obtained from the TCAF solution (Chakrabarti & Titarchuk 1995).

2 OBSERVATION AND ANALYSIS

For this investigation, we chose hard intermediate state (χ class) data which is very similar to hard and hard intermediate state of transient sources in respect of QPO evolution and spectral variations (Klein-Wolt et al. 2002; Pal et al. 2013). We analyzed two different χ class observations of GRS 1915+105 by *RXTE* in the period MJD 50270 - 50315 and MJD 50720 - 50760. We termed them as χ set-1 and χ set-2 respectively. We limit our analysis to observations when low frequency QPOs (LFQPOs) are observed. We used Good Xenon, Event and Single Bit modes which contain high time resolution data for timing analysis, which was performed using the GHATS software¹, a customized IDL based timing package, which takes care of Poisson noise subtraction and dead-time correction (Zhang et al. 1995) of the FFT data. We produced Power Density Spectra (PDS) of light curve segments of 16s length in the energy band of 2-30 keV. We averaged them to obtain an average PDS for each set observation. The PDSs were normalized and converted to fractional squared RMS. The power spectra were then fitted with a combinations of Lorentzians (see, Nowak 2000) using XSPEC v 12.0. We also produce the PDS for different energy bands to study energy dependent fractional amplitude variations.

Fig. 1(a) and Fig. 1(b) shows the ASM light curve for χ set-1 and χ set-2 respectively. The gray diamonds in the top of each panel show the dates in which the PCA observation was made.

In our analysis, we produced time lag spectrum for each observation of χ set-1 & χ set-2 data. We divide the data into a few energy bands depending upon the availability of the channel groups. For χ set-1, the channel groups are: 0-13 (2.0-5.23) keV, 14-18 (5.23-7.07) keV, 19-25 (7.07-9.57) keV, 26-35 (9.57-13.17) keV, 36-49 (13.17-18.27) keV, 50-65 (18.27-24.38) keV, 66-89 (24.38-33.06) keV. For χ set-2, the channel groups are: 0-13 (2.0-5.23) keV, 14-19 (5.23-7.42) keV, 20-25 (7.42-9.57) keV, 26-35 (9.57-13.17) keV, 36-50 (13.17-18.64) keV, 51-67 (18.64-24.87) keV, 68-89 (24.87-33.06) keV. The cross spectrum is defined as $C(j) = f_1^*(j) \times f_2(j)$, where f_1 and f_2 are the complex Fourier coefficients for the two energy bands at a frequency ν_j and here $f_1^*(j)$ is the complex conjugate of $f_1(j)$ (van der Klis et al. 1987). The phase lag between two band signals at Fourier frequency ν_j is $\phi_j = \arg[C(j)]$ and the corresponding time lag is $\phi_j/2\pi\nu_j$ (Uttley et al. 2014). We calculate an average cross vector C by averaging complex values over multiple adjacent 16s cross spectra and then finding the final value of time lag versus frequency. Following the method described in Reig et al. (2000), we calculate time lags at the QPO centroid frequency (ν_c) averaging over the interval $n\nu_c \pm FWHM$

¹ http://Astrosat.iucaa.in/~astrosat/GHATS_Package/Home.html

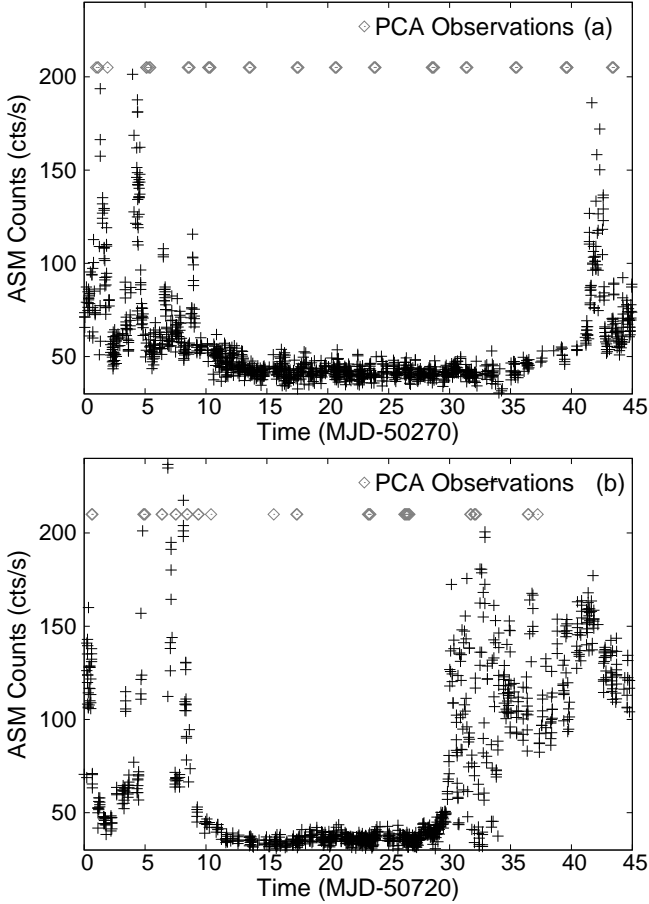


Figure 1. (a) ASM light curve during χ set-1 data, analyzed between MJD 50270 and MJD 50315. The gray diamonds represent the RXTE-PCA Observations of the days which were available in this period. (b) ASM light curve during χ set-2 data, analyzed between MJD 50720 and MJD 50760. The gray diamonds represent the RXTE-PCA Observations of the days which were available in this period.

for each energy bands mentioned above w.r.t. 2.0-5.23 keV energy band (Uttley et al. 2014). In all time lag spectra, positive lag values mean that hard photons are lagging soft photons. We found that dead time effects are negligible.

We have already introduced the Comptonizing Efficiency (CE) (see for detail, Pal & Chakrabarti 2014; Pal et al. 2013, 2011; Pal & Chakrabarti 2015) which is more accurate than hardness ratios (HR) since it is dynamically computed and the energy ranges are dynamically determined from the spectral fit. Normal HR comes from light curve and they do not need spectral information. The Comptonizing Efficiency (CE) is defined as the ratio of total number of power-law photons (N_{PL}) (defined as in Titarchuk (1994)) and the total number of soft (seed) photons (N_{BB}) from the standard disc model of (Makishima et al. 1986). The ranges of integration would be different for different spectrum since CE is not just a hardness ratio. The limits of energy range we chose is determined case by case as presented in Pal et al. (2013) and Pal & Chakrabarti (2014). Thus, the ratio, $CE = N_{PL}/N_{BB}$ can be calculated from the spectrum alone by fitting black body and power law com-

ponent but it has nothing to do with any specific accretion flow model (e.g., TCAF etc.) and it does not depend on the mass.

In the TCAF model, the POS solution has been successfully applied to study the evolution of QPO frequencies and to explain the variation of accretion flow geometry during the rising and the declining phases of the outbursts of a few transient BHCs, such as GRO J1655-40 (Chakrabarti et al. 2008, 2005), XTE J1550-564 (Chakrabarti et al. 2009), GX 339-4 (Debnath et al. 2010; Nandi et al. 2012), H 1743-322 (Debnath et al. 2013) and IGR J17091-3624 (Iyer et al. 2015), MAXI J1659-152 (Molla et al. 2016) but never applied to any persistent source such as GRS 1915+105. In the shock oscillation model of QPOs, the oscillation of X-ray intensity is actually due to the oscillation of the post-shock (CENBOL) region (Molteni et al. 1996; Chakrabarti & Manickam 2000). The physical reason for the oscillation of shocks is as follows: considering a phase during which the shock is receding, in the frame comoving with the shock, the upstream flow would appear to be faster, and the post-shock region downstream would therefore be hotter and would cool down faster. This reduction of post-shock pressure causes the shock to return towards the black hole, and the process will continue till it overshoots the equilibrium region and comes much closer. From the shock frame the incoming flow would be slower and the post-shock cooling diminishes and compressional heating pushes the shock outward. Thus these two opposite effects cause the shock to oscillate only if the cooling time scale and the compressional heating time scale (infall time scale) are similar. Thus what we observe is a resonance. Furthermore, by moving back and forth, the CENBOL expands and shrinks and the number of intercepted photons, and therefore the processed hard photon number is modulated. With a power-law cooling ((Molteni et al. 1996), (Chakrabarti et al. 2004)) this was demonstrated. With a dynamical cooling such as a strong outflow, (e.g., Ryu et al. (1997)) is present, which is true when the shock condition is not satisfied, the CENBOL oscillates. In outbursting sources, an enhancement of the accretion rate increases the local density and thus the cooling rate. The resulting drop of the post-shock pressure reduces the shock location and increases the oscillation frequency (Mondal et al. 2015) during the phase leading to a softer state. Once the resonance sets in, it would continue to be locked into resonance till accretion rates change considerably, causing evolution of QPOs as the object goes to softer and harder states respectively. Most interestingly, this condition allows one to obtain QPO frequency from the shock location or the size of the Compton cloud (CENBOL).

The location of the shock wave (X_s) is calculated from the observed QPO frequency (ν_{QPO}) as it is assumed that QPOs are generated due to the oscillations of the shock. The generated QPO frequency (ν_{QPO}) is proportional to the inverse of infall time (t_{infall} , i.e., matter crossing time from the shock location to the black-hole), i.e., $\nu_{QPO} \sim \nu_{s0}/t_{infall}$ where $\nu_{s0} = c/r_s = c^3/2GM_{BH}$ is the inverse of $1 r_s$ light crossing time of a BH of mass M_{BH} (Molteni et al. 1996), (Chakrabarti & Manickam 2000) and also

$$t_{infall} \sim RX_s(X_s - 1)^{1/2} \sim X_s^{3/2} \quad (1)$$

R is the shock strength ($= \rho_+/\rho_-$, i.e., ratio of the post-shock to pre-shock densities.) Here we used the fact that the infall

of matter in the post-shock region is slowed down by a factor of R . Thus, the QPO frequency according to this model, is $\nu_{QPO} \sim X_s^{-3/2}$. The time dependent shock location is given by,

$$X_s(t) = r_{s0} \pm vt/r_g, \quad (2)$$

where, r_{s0} is the shock location when t is zero, i.e., on the first day of observation and v is the velocity of the shock wave. The positive sign in the second term is to be used for an outgoing shock (when the spectral state is gradually becoming harder) and the negative sign is to be used for the in-falling shock (when the spectral state is gradually becoming softer). X_s is in units of the Schwarzschild radius $r_g = 2GM/c^2$ where, M is the BH mass and c is the velocity of light.

3 RESULTS

The Fig. 2(a,b) shows the evolution of QPO frequency as a function of days (MJD) from MJD 50271 to MJD 50315 and from MJD 50720 to MJD 50757 respectively for the χ set-1 and χ set-2. As obtained from data, in both the cases we observe the QPO frequency to be decreasing with time when the spectrum is gradually hardened and increasing with time after reaching a minimum value when the spectrum is gradually softened. The behavior is respectively similar to the declining and rising phases of an outburst. In χ set-1 observations, initially (MJD 50271 to MJD 50278), the QPO was stalling around ~ 4.18 Hz and it gradually decreases to 0.46 Hz (from MJD 50278 to MJD 50287) in nine days. Immediately, the QPO frequency starts to increase from 0.46 Hz (MJD 50287) to 6.14 Hz (MJD 50315.4) in 28 days. The dashed curve represents our fit with POS solutions (equations 1 and 2). We find that the shock is located at $\sim 134.8 r_g$ and it increases gradually till $\sim 563.0 r_g$ in ~ 9 days in the first (hardening) phase and move away to $\sim 104.0 r_g$ in the second (softening) phase. Depending on the rate of cooling in the post-shock region, which drives the movement of shock front, the shock may be accelerating or decelerating. Accordingly, the shock compression ratio R also varies as the shock moves in or out in the following way: $1/R \rightarrow 1/R_0 \pm \alpha(t_d^2)$, where R_0 is the compression ratio at the first day, t_d is the time in days and α is a constant that determines how the strength of the shock becomes stronger/weaker. α is negative when the spectrum is gradually becoming harder and the shock becomes stronger with time and positive when the spectrum is gradually getting softer and the shock becomes weaker with time.

In χ set-1 observations, Fig. 2(a), the shock was found to drift away with time till MJD 50287 when $\nu_{QPO} = 0.46$ Hz, $R = 1.538$ and the spectrum gets harder. It evolves as $\nu_{QPO} \sim t_d^{-0.7}$ and $X_s \sim t_d^{1.1}$ (since, $\nu_{QPO} \sim X_s^{-2/3}$). After that, the shock steadily moves in towards the black hole with almost constant velocity ($v_s \sim t_d^{0.1}$) and the spectrum gets softer. Similarly, for χ set-2 observations, Fig. 2(b), the shock was found to drift away from the black hole (from MJD 50720) with time till MJD 50735 when $\nu_{QPO} = 0.845$ Hz and $R = 1.538$ (the value is assumed equal to that derived from χ set-1. It evolves as $\nu_{QPO} \sim t_d^{-0.9}$ and $X_s \sim t_d^{1.4}$. Subsequently, the shock steadily moves in towards the black hole with almost constant velocity ($v_s \sim t_d^{0.4}$) and reaches

at $X_s = 390.0 r_g$ as the spectrum softens. A similar result was also found in XTE J1550-564 where the shock steadily receded away from the black hole with almost constant velocity ($v_s \sim t_d^{0.2}$) (Chakrabarti et al. 2009). We observed a stalling in the shock motion also in GRO J1655-40 (Chakrabarti et al. 2008). We find the QPO frequency to immediately increase as the shock front starts to drift in the reverse direction i.e., towards the black hole as we observed in XTE J1550-564 where we found a sudden increase of QPO frequency towards the black hole (Chakrabarti et al. 2009).

In χ set-1 observations during the phase when the spectrum gets softer (MJD 50287 to MJD 50315), the fit requires the shock to be drifted with a constant velocity $v_0 = 473.0$ cm s $^{-1}$ towards the black hole from $X_s = 563.0 r_g$ to $X_s = 104.0 r_g$. The shock location is observed to be time dependent according to the POS model which explains QPOs and it becomes weaker as it propagates towards the black hole. $R \rightarrow 1$ as $r \rightarrow r_g$. The time needed for the shock to disappear, $t_d \sim 28.0$ days and using the relation, $1/R \rightarrow 1/R_0 + \alpha t_d^2$, we obtained from fitting that $\alpha = 0.0015$ and $R_0 = 1.538$. Similarly during MJD 50735 to MJD 50746 of χ set-2 observations, the fit requires the shock (assumed $R_0 = 1.538$) to be drifted with a constant velocity $v_0 = 400.0$ cm s $^{-1}$ towards the black hole from $X_s = 390.0 r_g$, with $\alpha = 0.0019$. A similar behavior was also observed in XTE J1550-564 during the softening phase of the 1998 outburst where the shock was propagating with a constant speed $v_0 = 1981$ cm s $^{-1}$ and $\alpha = 0.022$ (Chakrabarti et al. 2009) towards the black hole.

Fig. 3(a) shows the variation of time lag of 5.23 – 7.07 keV photons w.r.t 2.0–5.23 keV photons with shock locations during the observations χ set-1. Fig. 3(b) shows the variation of time lag of 5.23 – 7.42 keV photons w.r.t 2.0 – 5.23 keV photons with shock locations during the observations χ set-2. Solid squares represent the data during the softening phase of QPO frequency and hollow squares represent the data during the hardening phase of QPO frequency for both χ sets of observations. Thus, we find a systematic variation of time lag with shock location (i.e., movement of the shock front) which in turn represents the variation of Comptonizing region (i.e., CENBOL size) during the rising and declining phases of the persistent source for two different χ sets of observations. A similar variation of time lag with shock location was also observed for the transient source XTE J1550-564 (Dutta & Chakrabarti 2016).

In Fig. 4(a), we plot the time lags of 5.23 – 7.07 keV photons (black dots) and 13.17 – 18.27 keV photons (gray triangles) w.r.t. 2.0–5.23 keV photons with QPO frequency in the χ set-1 observations. The fit of these curves yield the values of switching frequency ~ 2.66 Hz and ~ 2.08 Hz for the time lags of 5.23 – 7.07 keV and 13.17 – 18.27 keV photons w.r.t 2.0 – 5.23 keV photons respectively. In Fig. 4(b), we plot the time lags of 5.23–7.42 keV photons (black dots) and 13.17–18.64 keV photons (gray triangles) w.r.t. 2.0–5.23 keV photons with QPO frequency in the χ set-2 observations. Again, the fit of these curves yield the values of switching frequency ~ 2.77 Hz and ~ 2.26 Hz for the time lags of 5.23–7.42 keV and 13.17–18.64 keV photons w.r.t 2.0–5.23 keV photons respectively. We will discuss the implication of this in Sect. 4.

In Fig. 5, we plot the energy dependence of time lags for different energy band photons mentioned in time lag calcu-

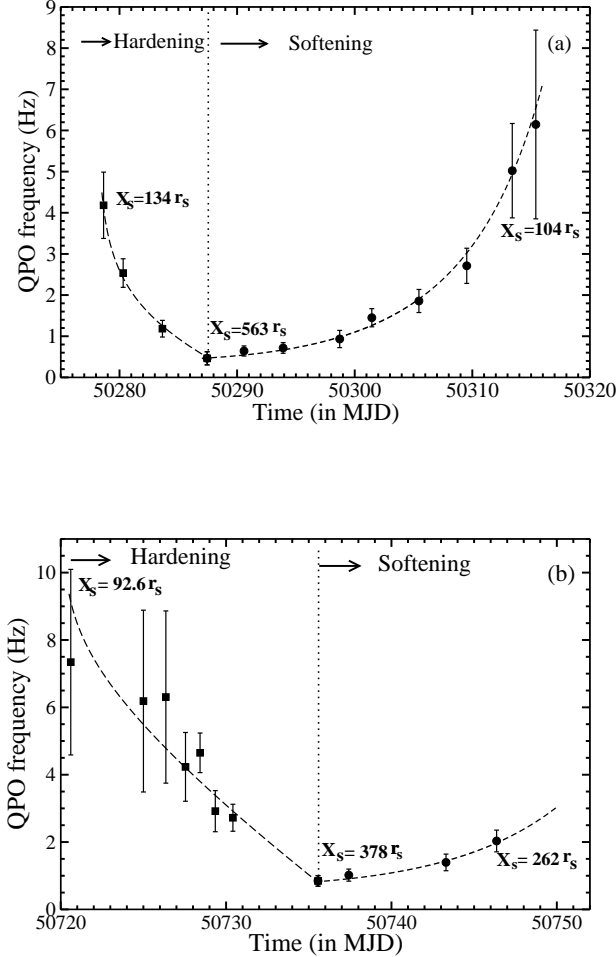


Figure 2. (a) Variations of QPO frequency with time (day) during the hardening and softening phases of χ set-1 with the fitted POS solution in TCAF model plotted. The shock moves at a constant speed ~ 473 cm/s towards the black hole. (b) Variations of QPO frequency with time (day) during the hardening and softening phases of χ set-2 with the fitted POS solution in TCAF model is plotted. Here, the shock moves at a constant speed ~ 400 cm/s during softening phase. The error bars are FWHM of the fitted Lorentzian in PDS. The dotted curve represents POS solution.

lation section w.r.t. 2.0 – 5.23 keV energy band at different QPO centroid frequencies (f_Q) for both χ set of observations. In Fig. 5(a), we show the energy dependent lag for five different QPO frequencies, viz. $f_Q = 1.18$ Hz (hollow red triangle), $f_Q = 1.96$ Hz (solid green square), $f_Q = 2.32$ Hz (hollow blue diamond), $f_Q = 2.58$ Hz (solid magenta triangle) and $f_Q = 5.52$ Hz (hollow cyan circle). During χ set-1 of observations for $f_Q \sim 2.32$ Hz, time lag is positive up to 8 keV. We find when $f_Q > 2.32$, time lag becomes negative (i.e., soft lag) at all energies. Time lag for QPO frequencies below 2.32 Hz are always positive in all observed energy

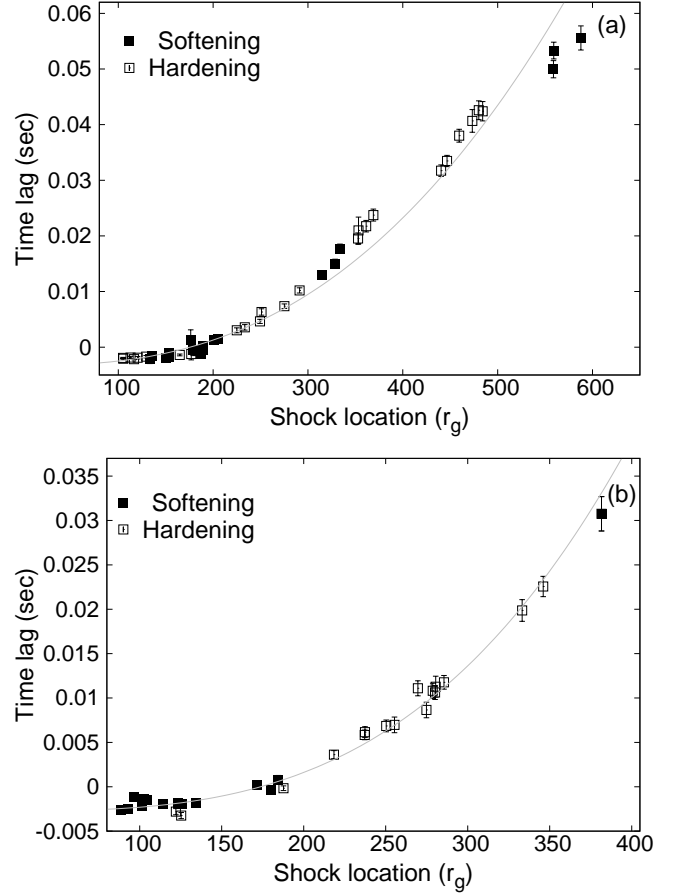


Figure 3. Variation of time lag with shock location (X_s) is plotted during the observations of χ state. Solid squares represent data during softening and hollow squares represent data during hardening. Time lag is calculated at the QPO centroid frequency (f_Q) integrated over the width equal to the FWHM of the QPO itself. (a) χ set-1 observations and (b) χ set-2 observations.

range. In fig. 5(b), we plot the same as in fig. 5(a) for the χ set-2 observations. We calculate this energy dependent lag for five QPO frequencies, viz., $f_Q = 1.48$ Hz (hollow red triangle), $f_Q = 2.03$ Hz (solid green square), $f_Q = 2.62$ Hz (hollow blue diamond), $f_Q = 2.92$ Hz (solid magenta triangle) and $f_Q = 6.31$ Hz (hollow cyan circle). During χ set-2 observations, for $f_Q = 2.62$ Hz, time lag is positive up to 6 keV. Again, we find $f_Q > 2.62$, time lag becomes negative (i.e., soft lag) at all energies. The time lags for QPO frequencies below 2.62 Hz are positive throughout all observed energy range. Time lag is always negative for the entire energy range when the oscillation frequency is greater than 2.62 Hz.

In Fig. 5(a,b), we show that the time lag monotonically increases with energy for QPO frequency ~ 1.18 Hz, but monotonically decreases from a frequency of ~ 2.3 Hz onward for χ set-1. Similarly, time lag monotonically increases with energy for QPO frequency ~ 1.48 Hz, but monotonically decreases from a frequency of ~ 2.62 Hz onward for χ set-2. A similar type of behavior was also observed for the transient source XTE J1550-564 (Dutta & Chakrabarti 2016). Physical processes producing high-energy photons im-

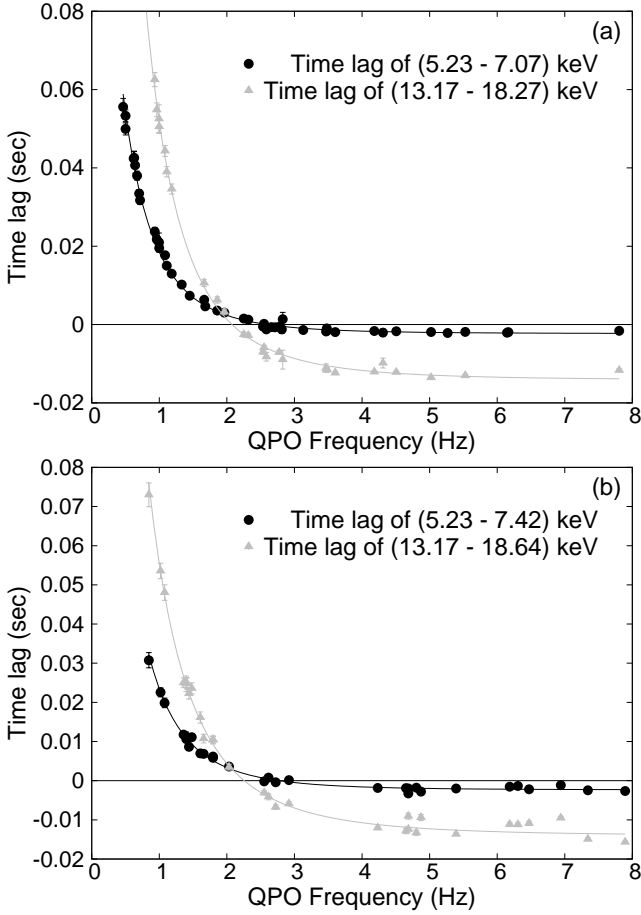


Figure 4. Time lag variation with QPO frequencies for different energy bands. We choose 2.0–5.23 keV as a reference energy band. (a) Black dots represent time lag of 5.23–7.07 keV energy band photons and gray triangles shows that of 13.17–18.27 keV energy band photons w.r.t the reference energy band during the χ set-1 observation. The fitted curves show that the time lag cross over frequency at ~ 2.66 Hz and ~ 2.08 Hz. (b) Black dots represent time lag of 5.23–7.42 keV energy band photons and gray triangles represent that of 13.17–18.64 keV energy band photons w.r.t the reference energy band during the χ set-2 observation. The fitted curves show that the time lag cross over frequency at ~ 2.77 Hz and ~ 2.26 Hz.

print energy-dependent time lags on the output radiation, therefore an energy dependence in the measured lags of high energy photons is naturally expected. Repeated Comptonization scatterings always produce longer time lags for hard photons. Similarly, the gravitational bending of photons (i.e., focusing of emitted photons) is energy and geometry dependent since higher-energy photons are expected to come from regions closer to a black hole (Chatterjee et al. 2017; Dutta & Chakrabarti 2016). Another major effect is the reflection of higher-energy photons which produce soft lag at high inclination angle (Dutta & Chakrabarti 2016).

In Fig. 6(a,b), the variation of fractional RMS amplitude for different QPO frequencies are plotted for χ set-1 and χ set-2 observations respectively. Here, we choose the QPO frequencies which are used in Fig. 2 (a,b) and symbols are used as in Fig. 5(a,b) for χ set-1 and χ set-2 ob-

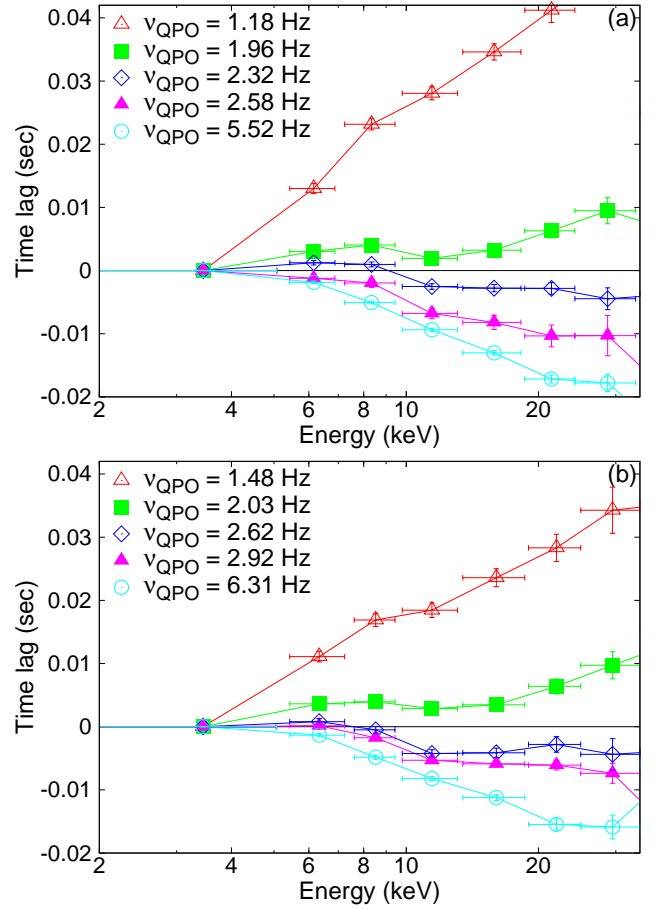


Figure 5. Energy-dependent time lag (w.r.t 2.0–5.23 keV) for different QPO centroid frequencies are plotted for χ set-1 (a) and χ set-2 (b) observations. We averaged the time lag over the width equal to the FWHM of the QPO itself. We calculated the time lag w.r.t the reference energy band w.r.t. 2.0–5.23 keV. The time lag switches its sign around QPO frequency of ~ 2.32 Hz (a) and ~ 2.62 Hz (b) for χ set-1 and χ set-2 observations respectively.

servations respectively. In Fig. 6(a), we find that the RMS amplitude increases with energy, reaches a maximum and then starts to decrease with energy. This implies that for both χ set observations, the mid-energy photons contribute to the quasi-periodic oscillations more than softer photons. We have already seen a similar behavior in other Galactic transient sources (Rao et al. 2000; Chakrabarti et al. 2008, 2009; Vadawale et al. 2001). The rms amplitude of the QPO decreases with increasing QPO frequency because a larger number of photons are taking part in oscillation at lower frequencies in comparison to those participating at higher QPO frequencies. According to the POS model the energy of the peak of the RMS spectrum should decrease with increasing QPO frequency, since the spectrum gets softer when the shock is closer to the black hole. Since the optical depth and temperature of the CENBOL limits the photon number at the higher end of the spectrum, we expect that the RMS power would go down at the highest energies. This is what we see in both the data sets.

Fig. 7 shows the variation of QPO frequency with the CE. The reason why this plot is important, is that the

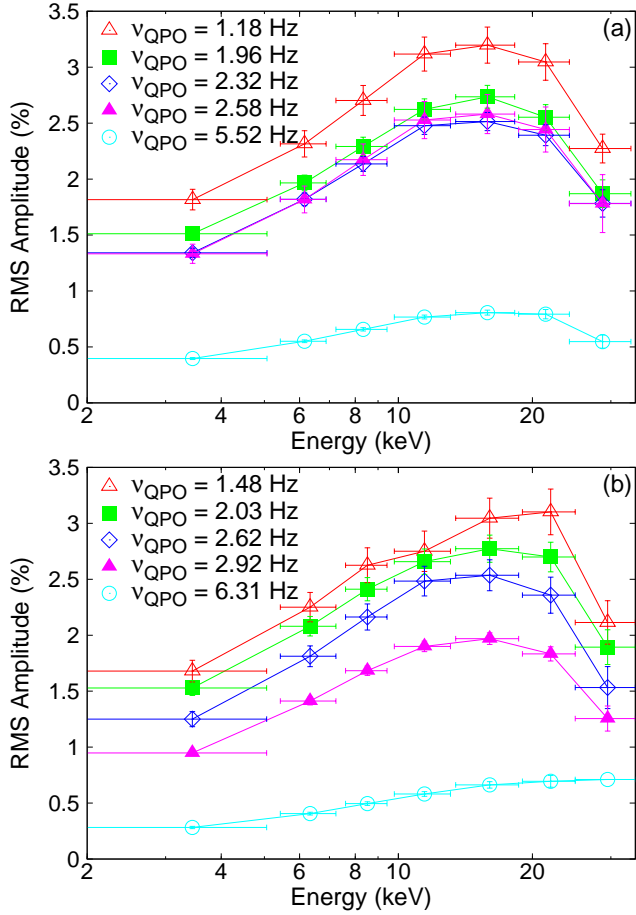


Figure 6. (a) Energy dependent RMS amplitude variation at different QPO frequencies. The energy range used here as in Fig. 5(a) for χ set-1 observation. (b) Energy dependent RMS amplitude variation at different QPO frequencies and the energy range used here as used in Fig. 5(b) for χ set-2 observation.

QPO frequency is correlated with the shock location and thus, the size of the CENBOL. CE represents the fraction of seed photons intercepted by the CENBOL and outflows, if any. During χ classes when sub-Keplerian halo accretion rate dominates, the geometry varies due to the movement of CENBOL boundary (shock location) and the formation of outflows from it. In order to compare the evolution, we superpose the data of the 1998 outburst of XTE J1550-564, reported in Fig. 6 of Pal & Chakrabarti (2014). We find for both the sources that the CE vs. QPO frequency evolution follows a similar track, independently of the fact that one is a persistent source and the other is a X-ray transient. The two sources have similar inclination (high) angle. We find for both the objects that the CE vs. QPO frequency evolution follows a similar track of evolution and independent of their nature.

Fig. 8 shows variation of time lag with CE for both χ set observations. In Pal et al. (2011, 2013), it was shown that when the Compton cloud or CENBOL is large the degree of interception of soft photons with CENBOL will also be greater. To quantify this, one requires the knowledge of the optical depth of the CENBOL as well as the fraction of photons intercepted by the CENBOL. We see this from

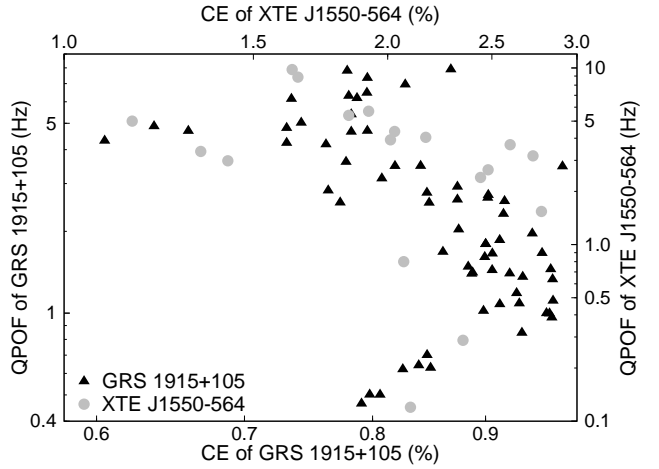


Figure 7. Black triangles show the variation of QPO Frequency with CE (%) observed in each of observation during the both χ set observations. Gray circles show the similar variation during 1998 outburst of XTE J1550-564. These points are taken from Fig. 6 of Pal & Chakrabarti (2014). Their evolutions are roughly along the same track.

our result: at very low QPO frequency ≤ 1 Hz, i.e., very large CENBOL size, CE is not at its maximum because the first scattering of photons takes place well inside the CENBOL. Once the CENBOL density is increased with accretion rates, the CE starts to go down with the CENBOL size. The larger size of the CENBOL at lower QPO frequencies is also confirmed by the fact that the time lags practically become positive at all energies, meaning that Compton up scattering dominates. This is seen in Fig. 8 for CE larger than $\sim 0.85\%$ and lag > 0 . In the lower branch $\sim 0.85 < CE < 1$, the optical depth of CENBOL is not high enough, but the outflow from CENBOL can also inverse Comptonize the photons, thus producing soft lags. In the upper branch $CE < 1$, the outflow continues to contribute to the time lag.

4 DISCUSSIONS & CONCLUSIONS

We present a coherent evolutionary picture of the persistent source GRS 1915+105 studying three main parameters, the type-C QPO frequency, its associated time lags and the Comptonizing Efficiency, in the framework of POS model. We analyzed two different sets of χ state observations and compared our results to those previously obtained from the study of the transient source XTE J1550-564. We find the evolution of QPO frequencies as a function of time from MJD 50271 to MJD 50315 and from MJD 50720 to MJD 50757 for the χ set-1 and χ set-2 data respectively. Within POS models, the initial decrease of QPO frequency as a function of time (declining QPO frequency and hardening of spectrum) is consistent with a shock steadily receding with almost constant velocity $v_s \sim t_d^{0.1}$ and $v_s \sim t_d^{0.4}$ for the χ set-1 and χ set-2 respectively. This variation is similar to what was observed in XTE J1550-564, ($v_s \sim t_d^{0.2}$) (Chakrabarti et al. 2009). Subsequent increase of QPO frequency (rising QPO frequencies and softening of spectrum) can be explained in terms of the shock moving towards the black hole with a constant velocity of $v_0 = 473.0 \text{ cm s}^{-1}$ and

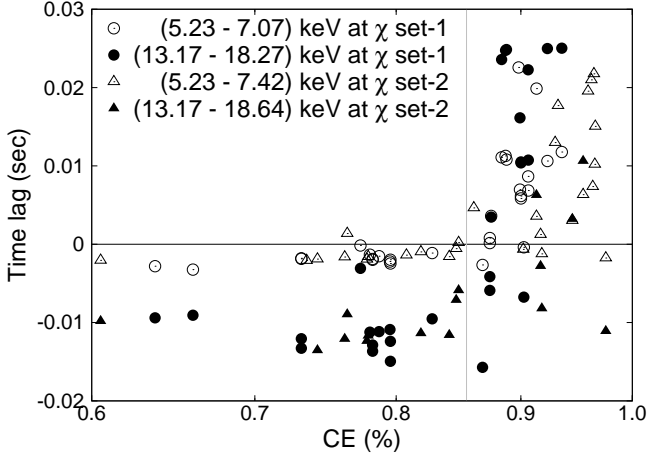


Figure 8. Hollow circles and solid circles show the time lag variation with CE (%) for (5.23-7.07) keV and (13.17-18.27) keV energy band photons respectively w.r.t (2.0-5.23) keV energy band photons during χ set-1 observation. Hollow triangle and solid triangle show the time lag variation with CE (%) for (5.23-7.42) keV and (13.17-18.64) keV energy band photons respectively w.r.t (2.0-5.23) keV energy band photons during χ set-2 observation.

$v_0 = 400.0 \text{ cm s}^{-1}$ for the χ set-1 and χ set-2 respectively. In XTE J1550-564, during a similar spectral variation phase, the shock was found to propagate with a much higher speed $v_0 = 1981 \text{ cm s}^{-1}$. This difference in velocity could be due to lower rate of cooling in GRS 1915+105. The fit also requires the shock to be time dependent in both the objects, and to become weaker as it propagates towards the black hole. Hence, the observed variations of QPO frequency with time resemble the variation in size of the CENBOL.

We find in both the sources that the time lag increases when the QPO frequency decreases, i.e., when the size of the Comptonizing region (i.e., CENBOL) increases, and that at a specific QPO frequency, i.e., at a specific size of the Comptonizing region, the lag changes from hard to soft (i.e., switches sign). We also find for both the objects that the CE vs. QPO frequency evolution looks similar, independently of the fact that one is a persistent source and the other is a transient source. CE represents the fraction of seed photons intercepted by the CENBOL and outflows, if any. During the χ state, when the sub-Keplerian flow rate dominates, the geometry varies due to movement of CENBOL boundary and the formation of outflows from it. At very low QPO frequency $\leq 1 \text{ Hz}$, i.e., when CENBOL is very large in size, CE is not maximum, because the first scattering takes place deeper inside the CENBOL where the optical depth ~ 1 . Then, the CE decreases with decreasing CENBOL size, i.e., increasing QPO frequency. The larger size of CENBOL at lower QPO frequencies is also confirmed by the fact that the time lags become positive at all energies when CE is larger than $\sim 0.85\%$ (Fig. 8). Again, at very low frequencies $\leq 1 \text{ Hz}$, we note that the CE increases with frequency (Fig. 7). This is possible only if the optical depth is increasing with decreasing CENBOL size (i.e., when accretion rate is also increasing) and/or outflow rate also increases. At higher frequencies, the trend is opposite: with the reduction of CENBOL size, the intercepted soft photon flux de-

creases, as expected normally. At higher frequencies, CENBOL becomes smaller as the spectrum becomes softer and the lag becomes negative, particularly for higher inclination sources, because of larger effects of reflection and focusing (Dutta & Chakrabarti 2016).

The spectrum of the lags at different QPO frequencies shows that for χ set-1 the hard lags increase monotonically with energy up to QPO frequency of $\sim 2.3 \text{ Hz}$ and for χ set-2, up to a QPO frequency of $\sim 2.62 \text{ Hz}$. This is similar to what we found in the transient source XTE J1550-564 (Dutta & Chakrabarti 2016). This behavior suggests that net observed time lag of the high-energy photons depends on the relative contribution of the different physical processes responsible for the high energy emission. Repeated scatterings and Comptonization always produce longer time lags for higher energy photons. The gravitational bending of photons (i.e., focusing of emitted photons) is an energy dependent process since higher-energy photons are expected to come from regions closer to a black hole (Chatterjee et al. 2017; Dutta & Chakrabarti 2016). For instance, high energy photons coming from the inner CENBOL in the opposite side would be focused towards the observer, but lower energy photons from farther out will not be focused. Other major effect is reflection of higher-energy photon which produce soft lags when the inclination angle is high (Dutta & Chakrabarti 2016) since the already delayed hard photons from CENBOL would be down scattered at the outer part of the disk. We therefore find that depending on the QPO frequency i.e., location of the shock, the lag could be positive or negative. This behavior suggests that the resultant or net time lag depends on the relative contribution from the different physical mechanisms by which they are generated. The fractional RMS amplitude is higher at medium energies for both χ set of observations but at very high energies rms goes down as the number of photons at high energy itself is reduced (at the turn-over energy) and also because they come from deep inside the CENBOL where oscillation is not as high and thus do not contribute to rms value.

With regard to the evolution of LFQPO properties and CE with time within the POS solution, the persistent source GRS 1915+105 and the transient source XTE J1550-564 do not show significant differences. Just as in the declining phase of an outburst the spectrum is hardened and QPO frequency is decreased, the first part of a χ state also shows exactly the same behavior. Similarly, just as in the rising phase of an outburst, the spectrum is softened and QPO frequency is increased, the second part of a χ state shows the same behavior. The shock location also decreases monotonically in the softening part of the χ state and exactly opposite behavior is seen in the hardening part of the state. We see that the geometry of the CENBOL evolves in the same way in the two types of sources. More generally, this conclusion might apply to any source belonging to the two different classes, with most of the observed differences being ascribable to different inclination angles. In other words, the apparently persistent class variable source such as GRS 1915+105 behaves as though it is made up of a large number of weak outbursts, nature of which is dictated by viscous processes which, in turn, decide the accretion rates.

ACKNOWLEDGMENTS

We acknowledge the Referee for helpful suggestions to improve the manuscript. We thank T. Belloni for providing the timing analysis software GHATS. B. G. Dutta acknowledges IUCAA for the Visiting Associateship Programme. P. S. Pal acknowledges the Post-Doctoral Fellowship at Sun Yat-sen University, China.

REFERENCES

- Böttcher M., Liang E. P., 1999, *ApJ*, **511**, L37
- Cabanac C., Henri G., Petrucci P.-O., Malzac J., Ferreira J., Belloni T. M., 2010, *MNRAS*, **404**, 738
- Cambier H. J., Smith D. M., 2013, *ApJ*, **767**, 46
- Chakrabarti S. K., Manickam S. G., 2000, *ApJ*, **531**, L41
- Chakrabarti S., Titarchuk L. G., 1995, *ApJ*, **455**, 623
- Chakrabarti S. K., Nandi A., Choudhury A., Chatterjee U., 2004, *ApJ*, **607**, 406
- Chakrabarti S. K., Nandi A., Chatterjee A. K., Choudhury A. K., Chatterjee U., 2005, *A&A*, **431**, 825
- Chakrabarti S. K., Debnath D., Nandi A., Pal P. S., 2008, *A&A*, **489**, L41
- Chakrabarti S. K., Dutta B. G., Pal P. S., 2009, *MNRAS*, **394**, 1463
- Chakrabarti S. K., Mondal S., Debnath D., 2015, *MNRAS*, **452**, 3451
- Chatterjee D., Debnath D., Chakrabarti S. K., Mondal S., Jana A., 2016, *ApJ*, **827**, 88
- Chatterjee A., Chakrabarti S. K., Ghosh H., 2017, *MNRAS*, **472**, 1842
- Choudhury M., Rao A. R., 2004, *ApJ*, **616**, L143
- Cui W., 1999, *ApJ*, **524**, L59
- Cui W., Zhang S. N., Chen W., 2000, *ApJ*, **531**, L45
- Debnath D., Chakrabarti S. K., Nandi A., 2010, *A&A*, **520**, A98
- Debnath D., Chakrabarti S. K., Nandi A., 2013, *Advances in Space Research*, **52**, 2143
- Debnath D., Molla A. A., Chakrabarti S. K., Mondal S., 2015, *ApJ*, **803**, 59
- Dutta B. G., Chakrabarti S. K., 2016, *ApJ*, **828**, 101
- Garain S. K., Ghosh H., Chakrabarti S. K., 2014, *MNRAS*, **437**, 1329
- Ghosh H., Garain S. K., Giri K., Chakrabarti S. K., 2011, *MNRAS*, **416**, 959
- Greiner J., Morgan E. H., Remillard R. A., 1996, *ApJ*, **473**, L107
- Haardt F., Maraschi L., 1993, *ApJ*, **413**, 507
- Hannikainen D. C., et al., 2005, *A&A*, **435**, 995
- Heil L. M., Uttley P., Klein-Wolt M., 2015, *MNRAS*, **448**, 3348
- Ingram A., van der Klis M., 2015, *MNRAS*, **446**, 3516
- Ingram A., Done C., Fragile P. C., 2009, *MNRAS*, **397**, L101
- Iyer N., Nandi A., Mandal S., 2015, *ApJ*, **807**, 108
- Klein-Wolt M., Fender R. P., Pooley G. G., Belloni T., Migliari S., Morgan E. H., van der Klis M., 2002, *MNRAS*, **331**, 745
- Li Z. B., Qu J. L., Song L. M., Ding G. Q., Zhang C. M., 2013, *MNRAS*, **428**, 1704
- Lin D., Smith I. A., Liang E. P., Böttcher M., 2000, *ApJ*, **543**, L141
- Makishima K., Maejima Y., Mitsuda K., Bradt H. V., Remillard R. A., Tuohy I. R., Hoshi R., Nakagawa M., 1986, *ApJ*, **308**, 635
- Markwardt C. B., Swank J. H., Taam R. E., 1999, *ApJ*, **513**, L37
- Martocchia A., Matt G., 1996, *MNRAS*, **282**, L53
- Miniutti G., Fabian A. C., 2004, *MNRAS*, **349**, 1435
- Mirabel I. F., Rodríguez L. F., 1994, *Nature*, **371**, 46
- Miyamoto S., Kitamoto S., Mitsuda K., Dotani T., 1988, *Nature*, **336**, 450
- Molla A. A., Debnath D., Chakrabarti S. K., Mondal S., Jana A., 2016, *MNRAS*, **460**, 3163
- Molla A. A., Chakrabarti S. K., Debnath D., Mondal S., 2017, *ApJ*, **834**, 88
- Molteni D., Sponholz H., Chakrabarti S. K., 1996, *ApJ*, **457**, 805
- Mondal S., Debnath D., Chakrabarti S. K., 2014, *ApJ*, **786**, 4
- Mondal S., Chakrabarti S. K., Debnath D., 2015, *ApJ*, **798**, 57
- Motta S. E., Casella P., Henze M., Muñoz-Darias T., Sanna A., Fender R., Belloni T., 2015, *MNRAS*, **447**, 2059
- Muñoz-Darias T., Coriat M., Plant D. S., Ponti G., Fender R. P., Dunn R. J. H., 2013, *MNRAS*, **432**, 1330
- Muno M. P., Morgan E. H., Remillard R. A., 1999, *ApJ*, **527**, 321
- Muno M. P., Remillard R. A., Morgan E. H., Waltman E. B., Dhawan V., Hjellming R. M., Pooley G., 2001, *ApJ*, **556**, 515
- Nandi A., Debnath D., Mandal S., Chakrabarti S. K., 2012, *A&A*, **542**, A56
- Noble S. C., Krolik J. H., Schnittman J. D., Hawley J. F., 2011, *ApJ*, **743**, 115
- Nowak M. A., 2000, *MNRAS*, **318**, 361
- Orosz J. A., Steiner J. F., McClintock J. E., Torres M. A. P., Remillard R. A., Bailyn C. D., Miller J. M., 2011, *ApJ*, **730**, 75
- Pahari M., Yadav J. S., Rodriguez J., Misra R., Bhattacharyya S., Pandey S. K., 2013, *ApJ*, **778**, 46
- Pal P. S., Chakrabarti S. K., 2014, *MNRAS*, **440**, 672
- Pal P. S., Chakrabarti S. K., 2015, *Advances in Space Research*, **56**, 1784
- Pal P. S., Chakrabarti S. K., Nandi A., 2011, *International Journal of Modern Physics D*, **20**, 2281
- Pal P. S., Chakrabarti S. K., Nandi A., 2013, *Advances in Space Research*, **52**, 740
- Payne D. G., 1980, *ApJ*, **237**, 951
- Pottschmidt K., Chernyakova M., Zdziarski A. A., Lubiński P., Smith D. M., Bezayiff N., 2006, *A&A*, **452**, 285
- Poutanen J., 2001, *Advances in Space Research*, **28**, 267
- Qu J. L., Lu F. J., Lu Y., Song L. M., Zhang S., Ding G. Q., Wang J. M., 2010, *ApJ*, **710**, 836
- Rao A. R., Naik S., Vadawale S. V., Chakrabarti S. K., 2000, *A&A*, **360**, L25
- Reig P., Belloni T., van der Klis M., Méndez M., Kylafis N. D., Ford E. C., 2000, *ApJ*, **541**, 883
- Remillard R. A., McClintock J. E., 2006, *ARA&A*, **44**, 49
- Ryu D., Chakrabarti S. K., Molteni D., 1997, *ApJ*, **474**, 378
- Schnittman J. D., Homan J., Miller J. M., 2006, *ApJ*, **642**, 420
- Smith D. M., Heindl W. A., Swank J. H., 2002, *ApJ*, **569**, 362
- Smith D. M., Dawson D. M., Swank J. H., 2007, *ApJ*, **669**, 1138
- Stella L., Vietri M., 1999, *Physical Review Letters*, **82**, 17
- Stella L., Vietri M., Morsink S. M., 1999, *ApJ*, **524**, L63
- Tagger M., Pellat R., 1999, *A&A*, **349**, 1003
- Titarchuk L., 1994, *ApJ*, **434**, 570
- Trudolyubov S., Churazov E., Gilfanov M., 1999, *A&A*, **351**, L15
- Uttley P., Cackett E. M., Fabian A. C., Kara E., Wilkins D. R., 2014, *A&ARv*, **22**, 72
- Vadawale S. V., Rao A. R., Chakrabarti S. K., 2001, *A&A*, **372**, 793
- Vierdayanti K., Sadowski A., Mineshige S., Bursa M., 2013, *MNRAS*, **436**, 71
- Wijnands R., Homan J., van der Klis M., 1999, *ApJ*, **526**, L33
- Wu K., et al., 2002, *ApJ*, **565**, 1161
- Yan S.-P., Ding G.-Q., Wang N., Qu J.-L., Song L.-M., 2013, *MNRAS*, **434**, 59
- Zdziarski A. A., Lubiński P., Gilfanov M., Revnivtsev M., 2003, *MNRAS*, **342**, 355
- Zhang W., Jahoda K., Swank J. H., Morgan E. H., Giles A. B., 1995, *ApJ*, **449**, 930
- van der Klis M., Hasinger G., Stella L., Langmeier A., van Paradijs J., Lewin W. H. G., 1987, *ApJ*, **319**, L13

This paper has been typeset from a \TeX/L\AA\TeX file prepared by the author.